

Effect of structure of PVDF membranes on the performance of membrane distillation

Hsu-Hsien Chang^{1a}, Chih-Hao Tsai¹, Hao-Cheng Wei¹ and Liao-Ping Cheng^{*1,2}

¹ Department of Chemical and Materials Engineering, Tamkang University, New Taipei City, 25137 Taiwan

² Energy and Opto-Electronic Materials Research Center, Tamkang University, New Taipei City, 25137 Taiwan

(Received September 24, 2013, Revised January 15, 2014, Accepted January 22, 2014)

Abstract. A series of microporous PVDF membranes were prepared by isothermal immersion-precipitation of PVDF/TEP casting dopes in both soft and harsh coagulation baths. Morphologies of the membranes' top surfaces were found to depend strongly on the bath strength, which could be controlled by the TEP content in the bath. By changing the bath gradually from pure water to 70% TEP, the top surface evolved from a dense skin-like (asymmetric) to a totally open porous morphology (symmetric). The latter structure could similarly be obtained by precipitation of the same dope in an alcoholic bath, e.g., 1-butanol. Membrane distillation processes to desalt sodium chloride aqueous solutions were conducted using various prepared membranes and two commercial microporous membranes, PTFE (Toyo, Japan, code: J020A330R) and PVDF (GE, USA, code: YMJWSP3001). The permeation fluxes were compared and correlated with the morphologies of the tested membranes.

Keywords: microporous membrane; PVDF; membrane distillation

1. Introduction

Membrane technology plays an important role over a broad range of separation processes due to energy saving, easy to operate, simple unit operation module, low maintenance cost, etc. Recently, water recycling and reuse have become an issue that attracts global attention. Making fresh water from sea water appears to be an attractive route that merits exploration. In fact, sea water desalination by membrane distillation method has been a subject of extensive research over the past decade. Until now, developing porous hydrophobic membranes for distillation process is still of great interest both to industry and academia. The concept of MD was originally proposed by Findley in the 60th (Findley 1967, Findley *et al.* 1969). The benefits of MD compared with other familiar separation processes include: (1) 100% (theoretical) rejection of ions, macromolecules, colloids, cells, and other non-volatiles; (2) lower operating temperatures than conventional distillation; (3) lower operating pressures than conventional pressure-driven membrane separation processes; (4) low demanding on membrane mechanical strength of membranes; and (5) reduced vapor spaces compared to conventional distillation processes (Adnan

*Corresponding author, Professor, E-mail: lpcheng@mail.tku.edu.tw

^a Ph.D., E-mail: greenchanghh@gmail.com

et al. 2012, Calabro *et al.* 1994, Essalhi and Khayet 2013, Gryta and Barancewicz 2010, Hou *et al.* 2012, Hou *et al.* 2012, Kuo *et al.* 2008, Lai *et al.* 2011, Lawson and Lloyd 1996b, 1997, Liao *et al.* 2013, Martinez and Rodriguez-Maroto 2008, Phattaranawik *et al.* 2003).

MD involves evaporation of an aqueous solution in contact with a porous surface of a water-repellent membrane, followed by transport of the generated vapor through the pores of the membrane, and finally condensation of the permeated vapor on the other side of the membrane. The presence of only gaseous phase inside the membrane pores is absolutely necessary for MD to succeed. This requirement should be warranted by the hydrophobic nature of the membrane. MD is performed in various prototypes that differ in the mode of permeate collection, the mechanism of mass transfer through the membrane, and the source of driving force. There are commonly four types of membrane distillation in use (Lawson and Lloyd 1997): direct contact membrane distillation (DCMD) (Adnan *et al.* 2012, Calabro *et al.* 1994, Essalhi and Khayet 2013, Gryta and Barancewicz 2010, Hou *et al.* 2012, Kuo *et al.* 2008, Lai *et al.* 2011, Lawson and Lloyd 1996b, Liao *et al.* 2013, Martinez and Rodriguez-Maroto 2008, Phattaranawik *et al.* 2003), air gap membrane distillation (AGMD) (Banat and Simandl 1994, 1998), sweeping gas membrane distillation (SGMD) and vacuum membrane distillation (VMD) (Lawson and Lloyd 1996a). Among these four types MD models, DCMD has the simplest configuration. The vapor generated from the hot side is condensed and merged into the cold water in direct contact with the membrane on the other side. The difference in vapor pressure between the hot and cold side pushes water molecules to diffuse through the membrane.

The performance of DCMD depends on the operation conditions (e.g., temperature, flow rate, concentration, etc.) and the membrane structure (e.g., porosity, pore size, thickness, hydrophobicity, etc.), which have been investigated in various aspects (Adnan *et al.* 2012, Calabro *et al.* 1994, Essalhi and Khayet 2013, Gryta and Barancewicz 2010, Hou *et al.* 2012, Kuo *et al.* 2008, Lai *et al.* 2011, Lawson and Lloyd 1996b, Liao *et al.* 2013, Martinez and Rodriguez-Maroto 2008, Phattaranawik *et al.* 2003). For example, Phattaranthe *et al.* analyzed their system based on a model that accounted simultaneous heat and mass transfer, and found that the effect of mass transfer on heat transfer rate was negligible even for high mass transfer convection cases (Phattaranawik *et al.* 2003). Lai *et al.* treated commercial PTFE membranes with plasma to enhance the membranes' surface hydrophilicity, by which significant improvements on the permeation fluxes were attained (Lai *et al.* 2011). Using a resistant-in-series model, Martinez *et al.* (2008) investigated the effects due to membrane thickness reduction, and claimed the existence of a critical thickness that maximized the permeation flux (Martinez and Rodriguez-Maroto 2008). Adnan compared the performance of PTFE membranes from different commercial sources, and correlated the results with the microstructure-related parameters, such as pore size, porosity, tortuosity, etc. (Adnan *et al.* 2012).

The effects of membrane structure on MD performance are less reported in the literature; particularly, for the case of membranes with similar cross section but different pore size and porosity on the top surface. The latter factors appear to be influential and merit exploration. In the present research, microporous PVDF membranes with such morphological features were prepared by non-solvent induced phase separation from the water/TEP/PVDF system (Lin *et al.* 2006). The membranes possess bi-continuous cross sections packed by interlinked crystallites coexisting with continuous porous channels. And their top surfaces vary from dense to partially open and then totally open structures. These membranes together with a commercial PVDF and a commercial PTFE membrane were tested on DCMD processes for desalination of NaCl(aq). Their performances were compared and correlated to the morphological factors.

2. Experimental

2.1 Materials

Poly(vinylidene fluoride) (PVDF) polymer (Kynar 740, Elf Atochem; intrinsic viscosity = 0.881 dL/g, $M_n = 254000$ g/mole) was supplied by Elf Atochem Inc. Triethylphosphate (TEP, Acros, reagent grade, $d = 0.944$ g/ml) and distilled and de-ionized water were used, respectively, as the solvent and non-solvent for membrane formation. 1-butanol (Reidel-de Haen, reagent grade, $d = 0.81$ g/ml) was used as the non-solvent. All materials were used as received.

2.2 Membrane preparation

PVDF membranes were prepared in the form of a flat sheet by the isothermal immersion-precipitation method (Akbari *et al.* 2012, Cheng 1999, Lin *et al.* 2006, Pang *et al.* 2011, Wang *et al.* 2009, Zhang *et al.* 2008, Zhang *et al.* 2012). First, PVDF was dissolved in TEP at 80°C on a roller to form a 20wt% homogeneous solution. This solution was held at room temperature for 1 h., and then cast on a glass plate using a casting device with a clearance of 400 μm . Following casting, the solution was immersed in a nonsolvent coagulant, which can be water, TEP aqueous solution, or 1-butanol, to induce polymer precipitation. The formed nascent membrane was removed from the glass plate and soaked in a series of non-solvents (typically 2-propanol followed by hexane) to extract residual TEP or 1-butanol. Subsequently, the membrane was press-dried between sheets of filter papers at 50°C. The preparation conditions for various membranes are listed in Table 1.

2.3 Characterization

The formed membranes were characterized by the following methods:

Table 1 Preparation conditiona and properties of PVDF membranes

Code	Bath TEP content (%)	Thickness (μm)	Bulk porosity (%) ^b	Bottom porosity (%) ^c	Top porosity (%) ^c	Contact angle (degree)	
						Top	Bottom
MW	0	125	66 \pm 5	65 \pm 2	0	82.9 \pm 0.5	104.2 \pm 0.8
M50	50	152	71 \pm 4	66 \pm 5	15 \pm 4	92.7 \pm 2.3	106.6 \pm 7.2
M70	70	183	80 \pm 3	66 \pm 4	50 \pm 6	111.4 \pm 4.4	110.2 \pm 2.3
MB	1-butanol	195	80 \pm 1	63 \pm 4	53 \pm 5	112.8 \pm 3.6	108.2 \pm 4.7
PVDF-C ^d	-	116	62 \pm 6	43 \pm 3	26 \pm 4	103.5 \pm 4.5	102.6 \pm 6.1
PTFE ^e	-	129	80	substrate	63 \pm 5	135.3 \pm 5.7	substrate

^a Dope: 20wt% PVDF in TEP.

^b Calculated based on the density of PVDF (1.78 g/cm³), the measured mass and thickness of the membrane.

^c Based on the image analysis by Image-Pro Plus version 6.

^d GE osmonics, USA, pore size 0.3 μm .

^e Advantec MFS, Inc. (Advantec Toyo), Japan, Hydrophobic PTFE w/ supported PP net, pore size 0.2 μm , 330 mm, J020A330R 1/pk

- (1) Morphologies of the membranes were observed using a field emission scanning electron microscope (FESEM, Leo 1530, Carl Zeiss, Oberkochen, Germany). A piece of membrane sample was vacuum-dried and then attached to a sample holder by conductive copper tapes. The cross section of the membrane was obtained by fracturing the membrane in liquid nitrogen. Silver paste was applied at the edges of the sample to enhance electronic conductivity. Then, the sample was sputtered with a thin layer (~2 nm) of Pt-Pd alloy and observed under a low acceleration voltage, 2 kV, by means of an in-lens detector. The pore and particle sizes in the SEM photographs were measured based on the calibrated scale. The surface porosity (fraction of pore area on the top or bottom surface) was measured using the software, Image-Pro Plus version 6.
- (2) The bulk porosity of the membrane was determined by the following equation (Lin *et al.* 2006).

$$\text{Porosity}(\%) = \frac{(V_m - V_p)}{V_m} \times 100\%$$

where V_m is the bulk volume of the membrane and V_p is the volume of the polymer. V_m was obtained by multiplying the membrane area by its thickness, which was measured by a thickness gauge. V_p can be calculated by W_m/ρ_p , where W_m is the weight of the membrane and ρ_p is the density of polymer. The value of $\rho_p = 1.78 \text{ g/cm}^3$ for PVDF, as is provided by the supplier.

- (3) The contact angles of the membranes were measured by a contact angle/surface tension analyzer (FTA 125, VA, USA) at room temperature. A drop of water (2 μl) was deposited on the surface of the membrane. Image of the water droplet was taken and the contact angle was measured from shape analysis. To ensure reliable data being obtained, 5 measurements at different locations of the membrane surface were taken and the average value was reported.

2.4 DCMD operations

The DCMD setup for our experiments, as shown schematically in Fig. 1, consists of three key parts: the cold water loop, the hot water loop, and the membrane modules. In the hot water loop flows the feed solution, which is composed of 3.5wt% sodium chloride dissolved in pure water. Temperature of the feed was controlled at a constant value of 30, 40, or 50°C by an external thermostat. In the cold water loop, distilled water at 20°C was circulated to condense and carry away the permeated vapor. In each loop, a large reservoir was installed to ensure steady concentration and temperature being maintained during operation. The membrane module comprises two compartments, donor and receptor. The PVDF membrane to be tested was tightly held (sealed with silicone rubber) between these two compartments. Several membrane modules can be linked in parallel to increase the total permeation flux; e.g., a set composed of 3 modules is shown in Fig. 1. Two independent pumps were used to circulate the liquids in the loops with a flow rate of 0.7 L/min. Desalted water product was collected via an overflow design in the cold water loop. The effective area of the membrane in each module was 25 cm². After the flow rates and the temperature reached a stable constant value, which took ~2-3 h of operation time, samples were collected for subsequent salt rejection and permeation flux measurements. The time for each collection was 1 h, and over the period of 24 h., five collections were made and the results compared.

The obtained rejection ratio, R , was defined as

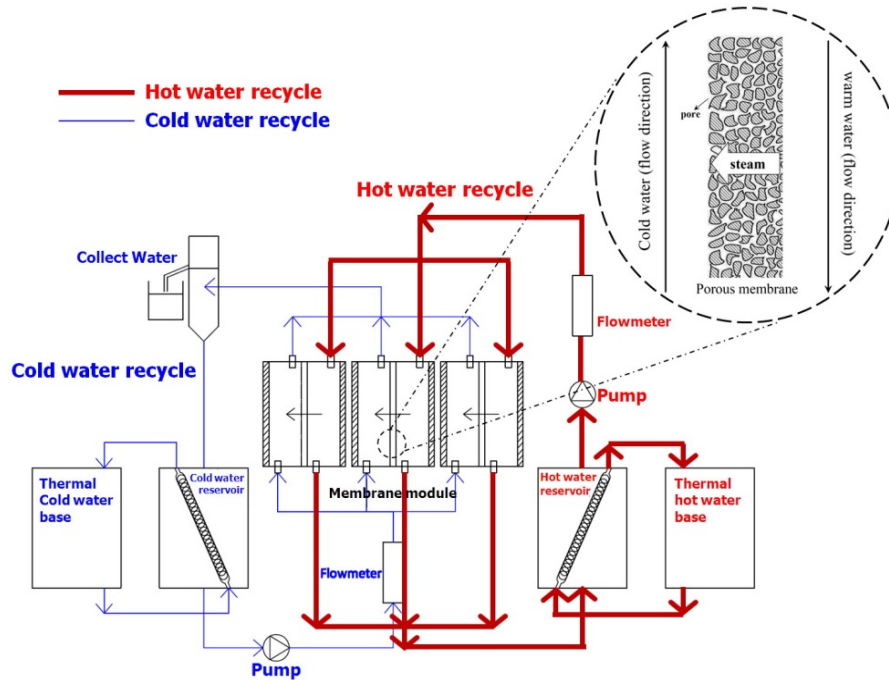


Fig. 1 The schematic representation of DMDC setup

$$R = \frac{C_d - C_r}{C_d} \times 100\%$$

where C_d and C_r denote the sodium chloride concentration in the donor and receptor side, respectively (Hou *et al.* 2012, Kuo *et al.* 2008).

3. Results and discussion

Microporous PVDF membranes were prepared by isothermal immersion-precipitation of PVDF/TEP casting dopes in coagulation baths of different TEP contents. Fig. 2 shows the overall cross sectional images of three representative membranes, MW, M50, and M70. All of them exhibit a relatively uniform porous morphology with little evidence of cellular pore formation. The high magnification images of the membranes, as shown in Fig. 3, illustrate the fine structure of the membranes. MW is composed of stick-like crystal elements (often termed axilites in the literature) that interlock into a continuous matrix intertwining with the continuous network of pores. Such ‘bi-continuous’ morphological feature is associated with the usage of an incipient dope (i.e., a dope in the metastable state that contains huge amount of pre-nucleation embryos) (Chang *et al.* 2013, Lin *et al.* 2006a, Lin *et al.* 2006). As a result, crystallization would take place rapidly upon concentration fluctuation during immersing of the dope into the bath. The detailed description of the formation mechanism can be found in the literature (Chang *et al.* 2013, Lin *et al.* 2006a, b, Lin

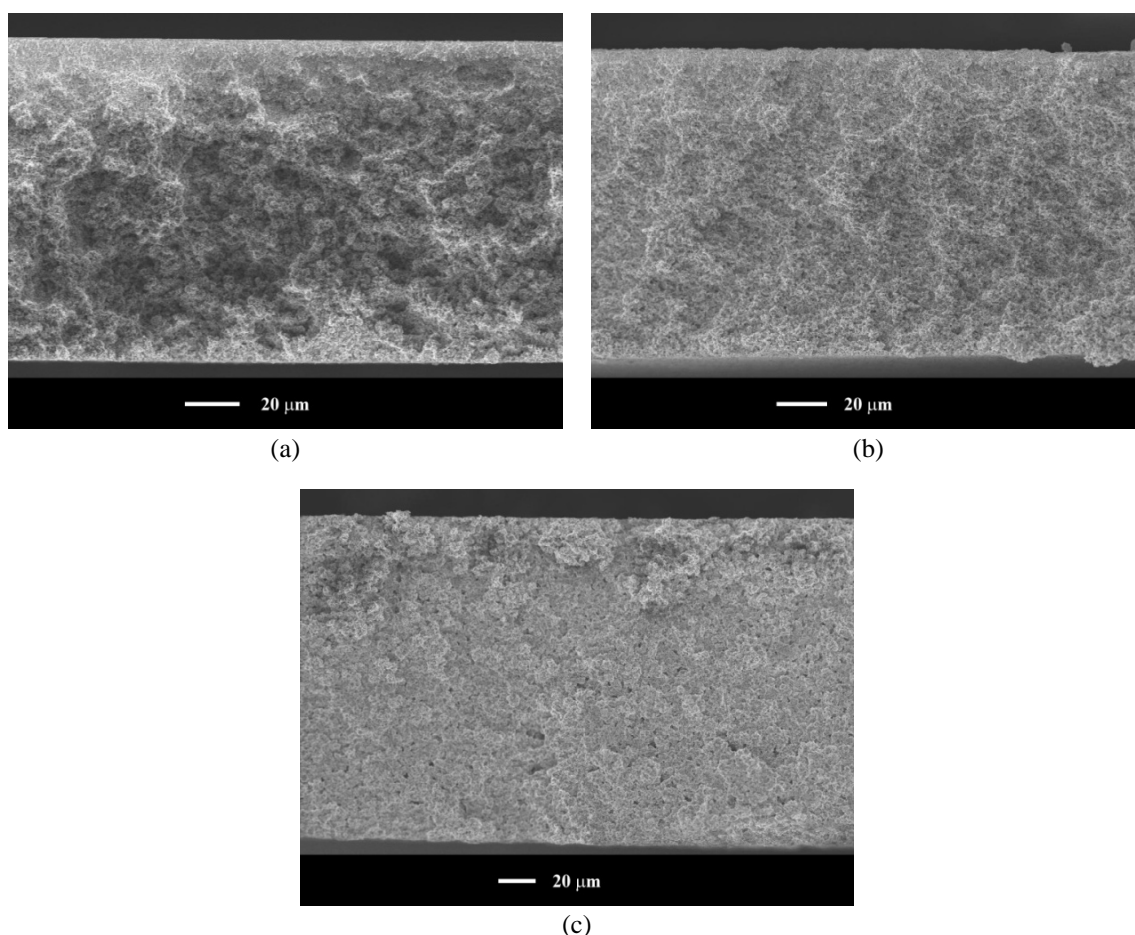


Fig. 2 The overall cross-section morphologies of microporous PVDF membranes: (a) MW; (b) M50; (c) M70

et al. 2006). Likewise, the membranes M50 and M70 exhibit the bi-continuous morphology, c.f., Figs. 3(b) and 3(c). However, it is noted that the shape of the crystallites becomes more and more sheaf-like with increasing TEP content in the bath. In other words, the population density of nuclei is lower (or equivalently the crystal size in the membrane is larger) when the dope is precipitated in a more concentrated bath. Because larger particles tend to pack into structure with larger pores, the pore size of M70 ($6.1 \mu\text{m}$, based on image analysis) is expected to be larger than the other two membranes ($M50 = 3.3 \mu\text{m}$, $MW = 1.7 \mu\text{m}$), agreeing with the SEM images shown in Fig. 3. The measured porosity data of the membranes are listed in Table 1. They increase slightly from MW to M70. Specifically, the porosity of M70 reaches a value as high as 80%, making it a good candidate for membrane distillation process, for which high permeation fluxes are desirable.

The top surface morphologies of the above three PVDF membranes are shown in Fig. 4. Membrane MW has a non-porous skin layer that is composed of densely packed sheaf-like spherulitic elements, cf. the high magnification view (Chang *et al.* 2013, Lin *et al.* 2006). Such

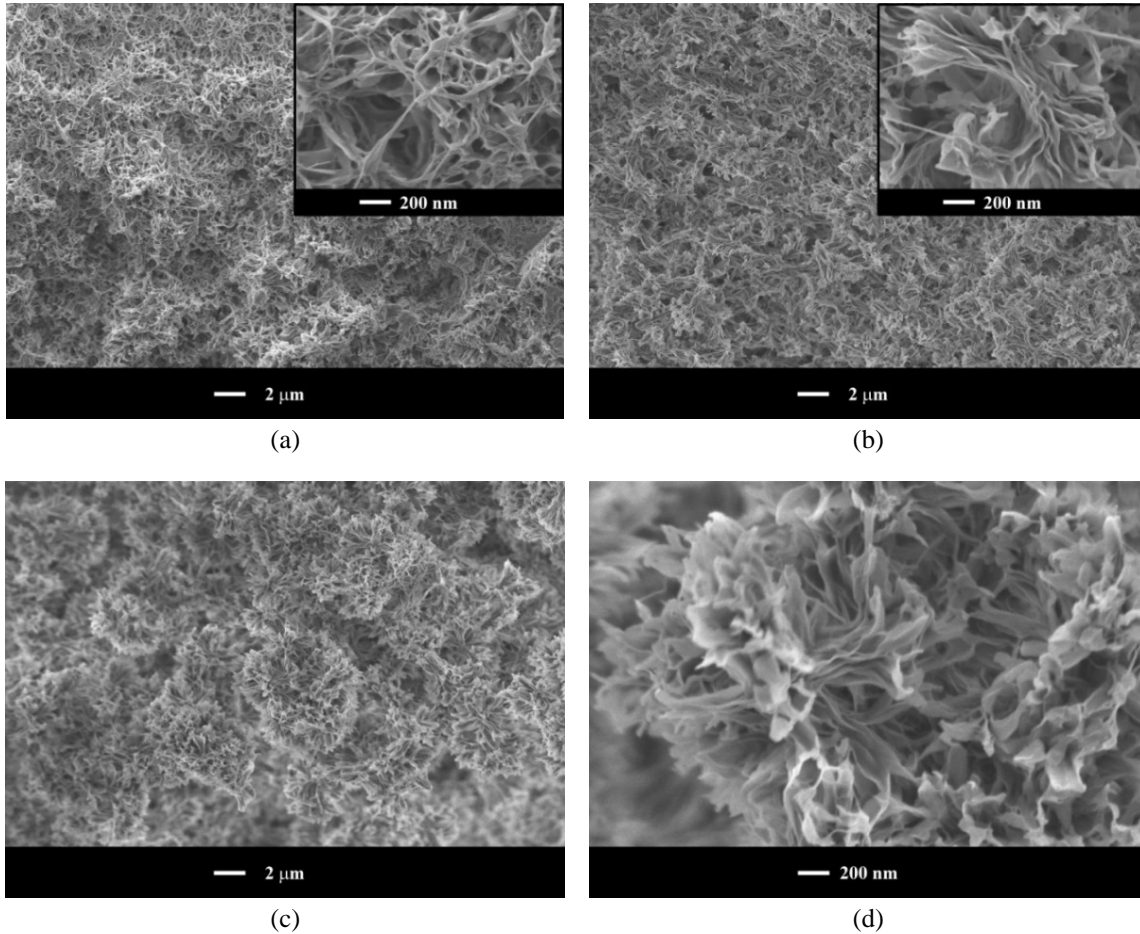


Fig. 3 The cross-section morphologies of microporous PVDF membranes: (a) MW (inset is the high magnification image); (b) M50 (inset is the high magnification image); (c) M70; (d) the high magnification image of the membrane (c)

surface layer appears to be impermeable to water molecules in ordinary low pressure separation processes such as microfiltration (MF) and MD. In contrast, the top surface of the membrane M70 is skinless with bi-continuous porous structure resembling that of the cross-section. The membrane M50 exhibits a morphology being intermediate of MW and M70; it has a rugged and slightly porous surface, containing sporadic micron-sized crevices whereby feed molecules may use entrances to the interior porous channels. The above morphological features are a direct reflection of the strength of the non-solvent coagulation baths. During precipitation in a harsh bath, such as water, a robust gel layer would form on the top surface due to the rapid boost of polymer concentration at the membrane-bath interface (Lin *et al.* 2006b, Lin *et al.* 2006). This gel layer solidifies subsequently by means of crystallization and/or vitrification (amorphous, in case) to become a dense skin. On the other hand, if a very soft bath (e.g., 70% TEP aqueous solution) is employed, the top gel layer would be soft, which is easily broken-up by the phase separation

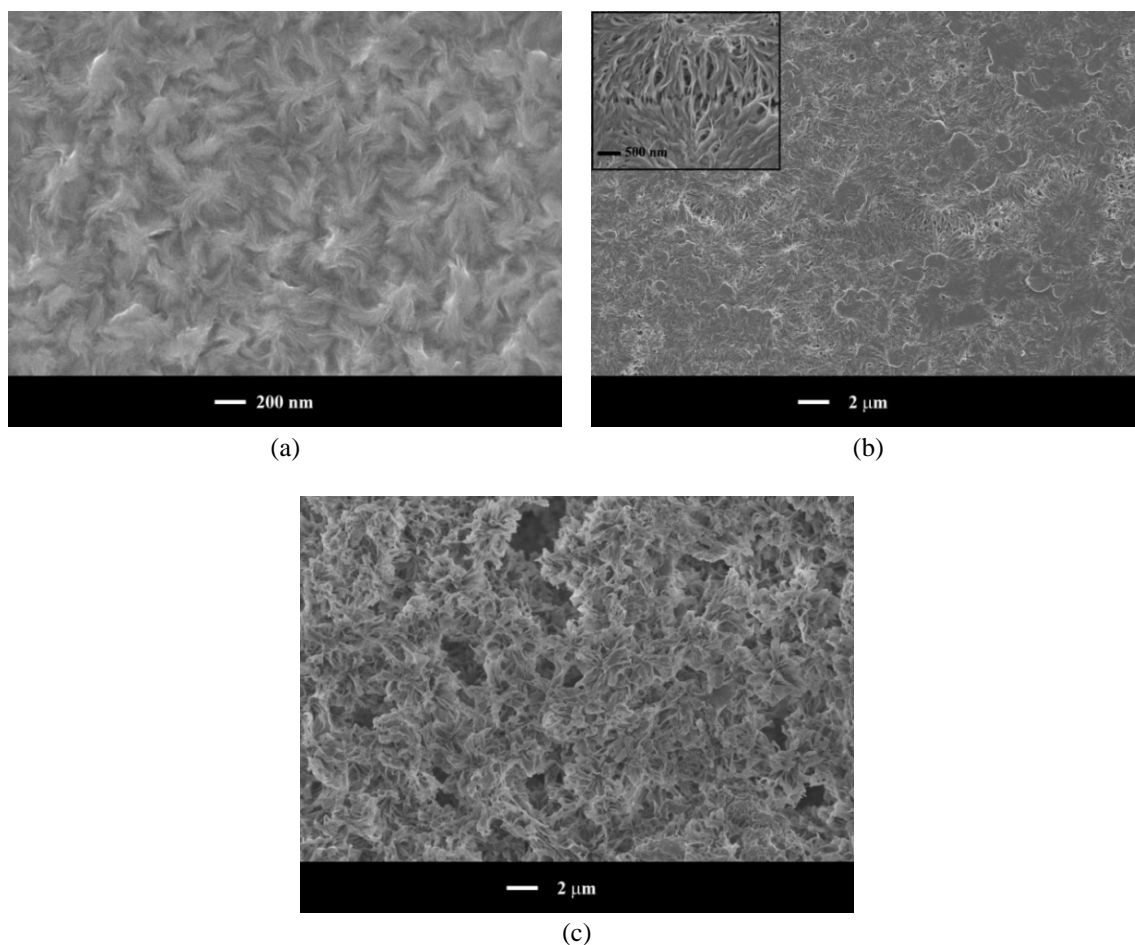


Fig. 4 The top surface morphologies of microporous PVDF membranes: (a) MW; (b) M50; (c) M70

events taking place in this region. The tensile strengths of the membranes decreased with increasing TEP contents in the nonsolvent bath, as shown previously (Lin *et al.* 2006). The tensile strength of the membrane MW reached 5.7 MPa, which could be attributed to the denser skin and less porous cross-section that it possessed. For the membrane M70, with a skinless symmetric morphology, the tensile strength was 1.1 MPa.

The bottom surfaces of the membranes bear a similar morphology to their cross sections. For example, as illustrated in Fig. 5, M70 has a bottom surface composed of sheaf-like spherulites of the size $\sim 2\text{-}4\ \mu\text{m}$, just as those shown in Fig. 3(c). However, some flattened features on the spherulites' surface are noted, which are derived from 2-D growth of the spherulites pressing against the smooth glass plate (Chang *et al.* 2013, Lin *et al.* 2006b). Apart from the flattened feature, this membrane may be termed “symmetric” with all dimensions sharing the same porous structure (in particular, the top surface is discernible from the cross section). As all micro-pores intertwine into continuous channels across the whole cross section, it is expected that the

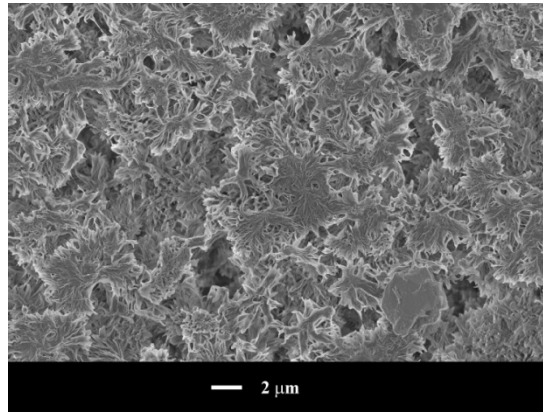


Fig. 5 The bottom surface morphology of the membrane M70

membrane will generate high permeation fluxes on common MD and MF processes. In addition to the 70% TEP(aq) solution, another soft bath, pure 1-butanol, was employed to prepare membranes (MB in Table 1) that bore a symmetric morphology similar to that of M70. The purposes are dual: (1) to show that similar structure can be formed even from baths consisting of totally different chemical species, and (2) that similar porous structure will give rise to close MD performance. The high resolution SEM images of MB are presented in Fig. 6; undoubtedly, the membrane is just like M70, being packed by sheaf-like spherulites into bi-continuous structure. Contact angle of the bottom and top surfaces of the membranes are listed in Table 1. Apparently, except for the top surface of MW, all other surfaces have contact angles high enough for MD processes.

The above prepared membranes and two commercial micro-porous membranes (PVDF and PTFE) were tested for their performances on membrane distillation processes. The commercial PVDF membrane (termed PVDF-C, hereinafter) was produced by GE (USA) with the code YMJWSP3001, whereas the PTFE was produced by Toyo (Japan) with the code J020A330R.

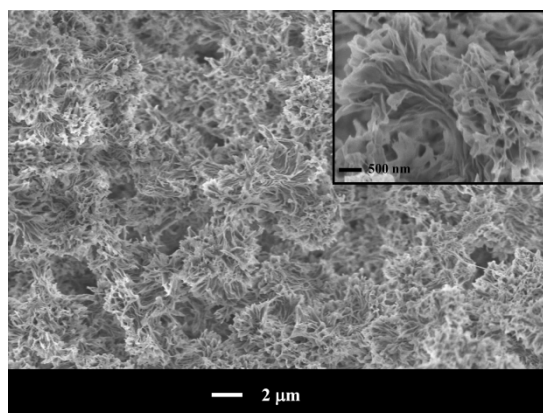


Fig. 6 The cross-section morphology of the membrane MB

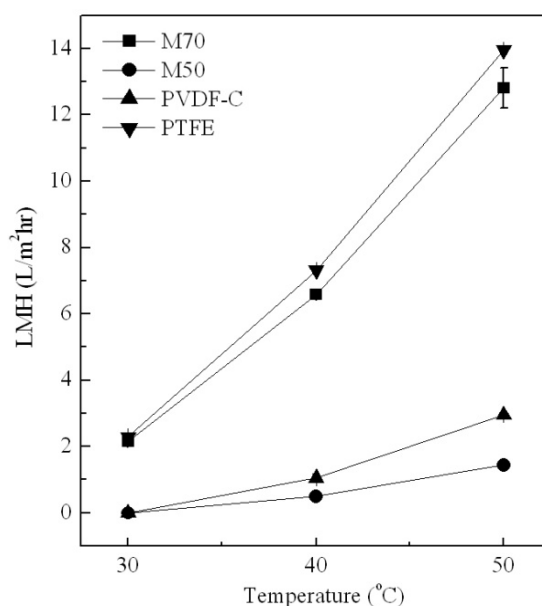


Fig. 7 Dependence of water permeation fluxes on feed temperature for different membranes

The feed solution of all MD experiments was 3.5wt.% NaCl(aq) solution, and on the permeate side distilled water was swept across the membrane to collect the condensed water. Fig. 7 and Table 2 summarize the permeation fluxes and rejection coefficients (R) for the tested membranes. The operation temperatures for the feed include 30, 40, and 50°C, while the permeate side was maintained at 20°C. For all cases, the rejection coefficients approach 100%, which is typical of MD processes having a nonvolatile solute in the feed (Hou *et al.* 2012, Kuo *et al.* 2008). This result also confirms good sealing of the cell, for otherwise even a small leakage would render the

Table 2 Water permeation fluxes and rejection coefficients of various membranes

Code	30°C		40°C		50°C	
	Flux (LMH) ^a	R (%) ^b	Flux (LMH) ^a	R (%) ^b	Flux (LMH) ^a	R (%) ^b
MW	-	-	-	-	-	-
M50	-	-	0.49 ± 0.03	99.9	1.44 ± 0.01	99.9
M70	2.16 ± 0.03	99.9	6.58 ± 0.15	99.9	12.8 ± 0.6	99.8
MB	-	-	-	-	12.3 ± 0.5	99.9
PVDF-C	-	-	1.05 ± 0.13	99.9	2.96 ± 0.03	99.9
PTFE	2.29 ± 0.03	99.9	7.32 ± 0.02	99.9	13.9 ± 0.3	99.9

^aLMH = L/m²hr.

^b R (%) = $[(C_d - C_r)/C_d] \times 100\%$, where C_d and C_r denote the sodium chloride concentration in the donor and receptor side, respectively

feed temperature, which is due to the increased water volatility. The vapor pressures of 3.5% NaCl rejection away from ~100%. As regards the fluxes, it is found that they increase with increasing water solution are 2.29, 4.16, 7.23, and 12.08 kPa at 20, 30, 40 and 50°C, which suggest a more pronounced increase of permeation flux at a higher temperature, consistent with the permeation fluxes at these temperatures. The flux of membrane MW is negligibly small (< 0.1 LMH, estimated) obviously because of the dense skin it possesses; cf. Fig. 5(a). The membrane PVDF-C has fluxes somewhat larger than M50, yet much smaller than M70, MB, and PTFE, which can be attributed to the porous structures, particularly the top surface, of these membranes. Fig. 8 shows the SEM micrographs of the membrane PVDF-C. The cross sectional view indicates an asymmetric structure that is mainly occupied by irregularly-shaped large pores (macrovoids). This interesting feature appears to be beneficial to vapor transport, for which Knudsen diffusion is expected to be insignificant.

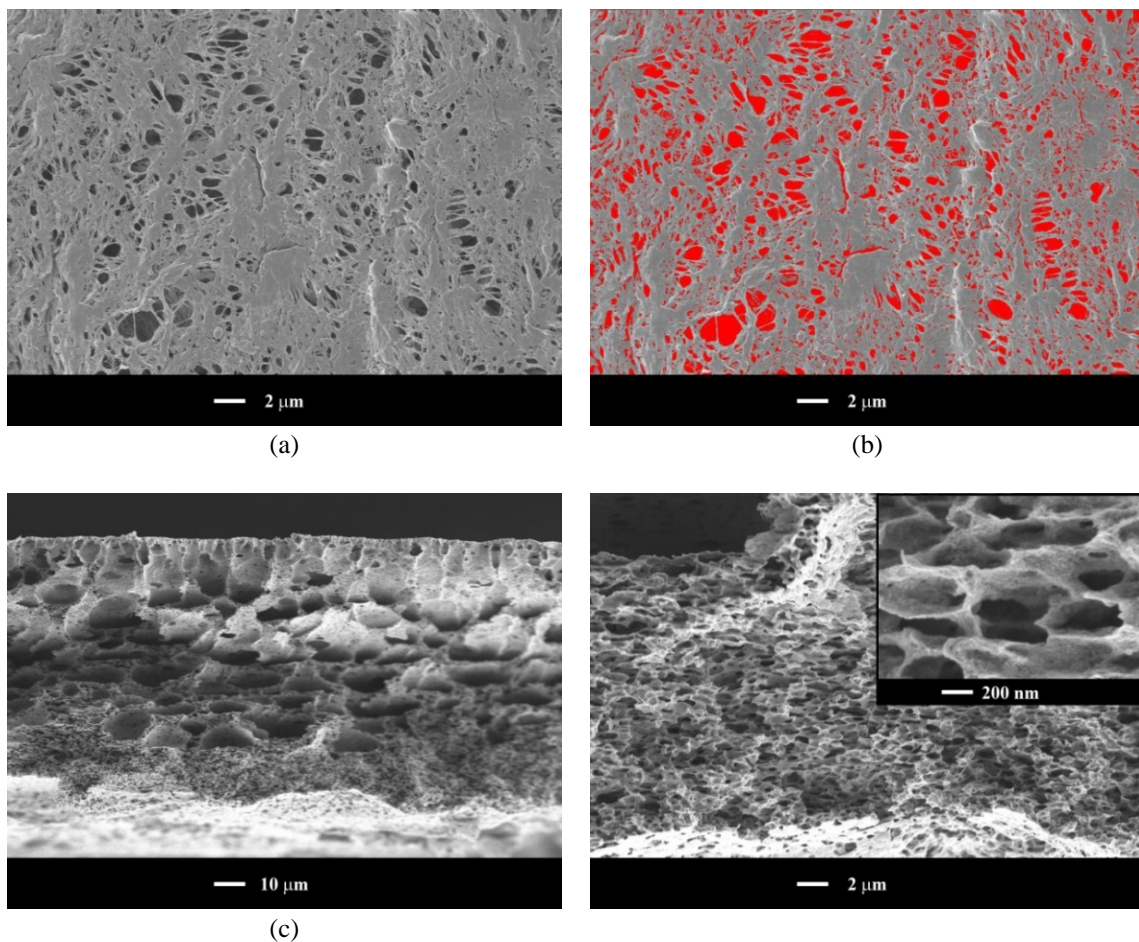


Fig. 8 The morphologies of the membrane commercial PVDF membrane (PVDF-C): (a) top surface; (b) image analysis graph of the top surface; (c) cross section; (d) the high magnification image of (c) near the bottom

However, towards the bottom surface region, cellular pores are frequently observed, as shown in Figs. 8(c) and 8(d), which if not totally open (interconnected) can inhibit the permeation of water molecules and lead to significant flux reduction. The top surface of the membrane contains pores of $\sim 1\text{-}2\ \mu\text{m}$ that allow entrance of water molecules. However, based on the image analysis shown in Fig. 8(b), these pores constitute only $\sim 26\%$ of the surface area, which is larger than that for M50 ($\sim 15\%$), yet much smaller than that for M70 ($\sim 50\%$), as shown in Fig. 9 (also referring to Table 2). Given the small top surface porosity and the frequent presence of cellular pores near the bottom surface, one can judge confidently that the permeation fluxes of PVDF-C would be much smaller than those of the membrane M70. For the latter membrane, water vapor can diffuse relatively easily through the large and porous channels across the membrane. As to the membrane M50, although the bi-continuous cross section and high porosity favor high flux, the barely porous top surface hinders water transport and renders the flux on the lower end. Membranes MB and M70 have very close permeation fluxes (12.3 and 12.8 LMH, respectively, with feed temperature at 50°C), which confirms the fact that these two membranes have similar structure and porosity.

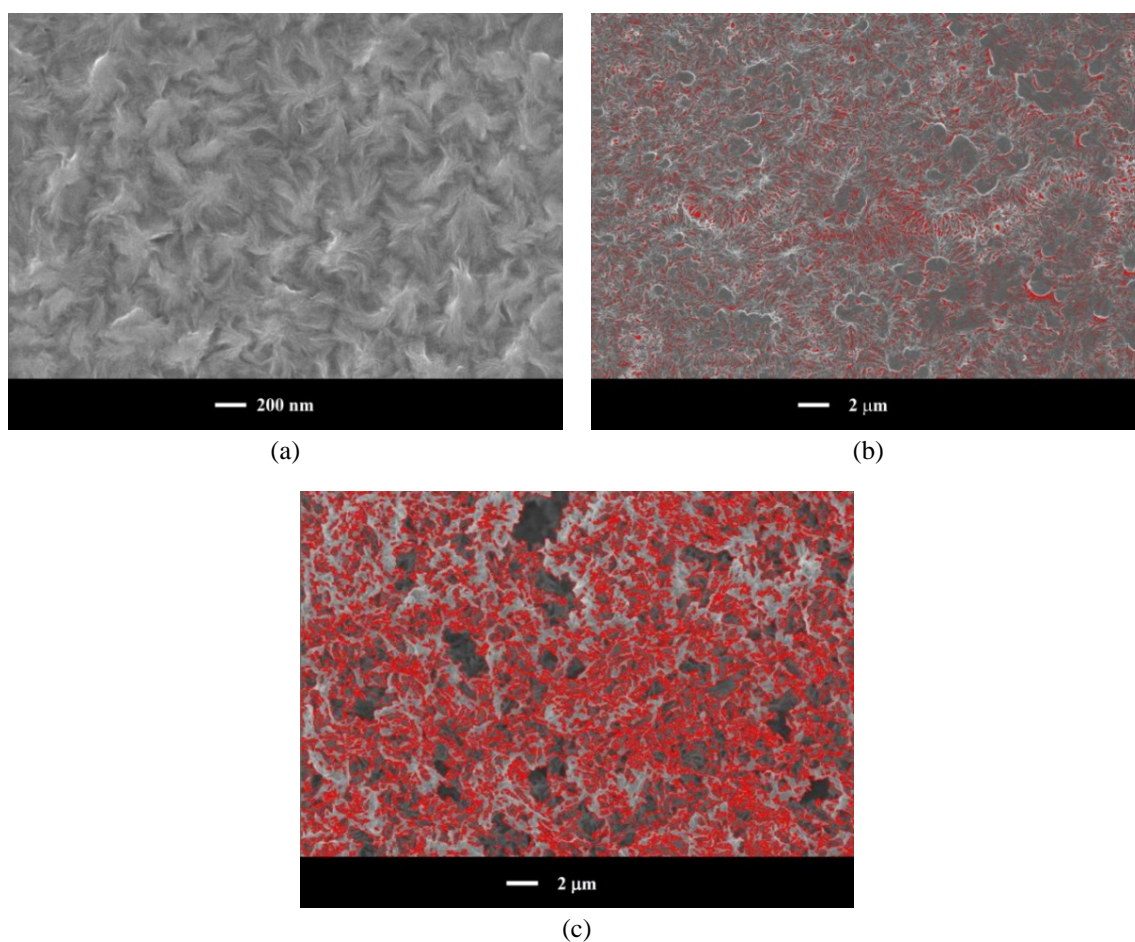


Fig. 9 The image analysis graph of the top surface: (a) MW; (b) M50; (c) M70

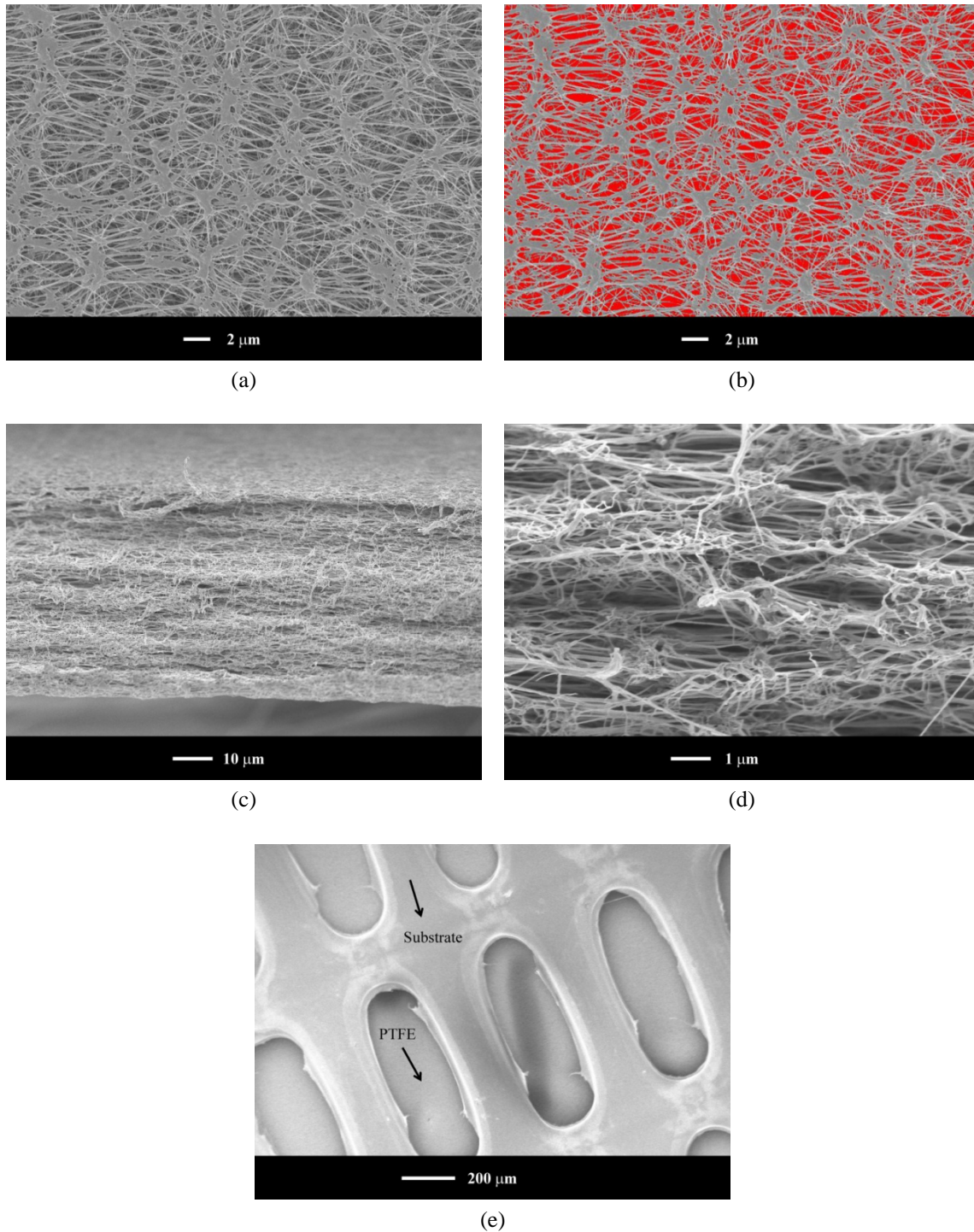


Fig. 10 The morphologies of the commercial PTFE membrane: (a) top surface; (b) image analysis graph; (c) cross-section; (d) high magnification of (c); (e) bottom substrate

PTFE has slightly higher permeation fluxes than M70 for all feed conditions, which can be understood by comparing the structure-related factors: pore size, bulk and surface porosities, membrane thickness, and bottom-support usage, of these two membranes. Fig. 10 shows the SEM micrographs of the PTFE membrane. As in M70, it has a symmetric structure with totally open pores interconnected into micro-channels distributed uniformly in the membrane. The pores are elongated reflecting the bi-axial stretching process for producing the membrane. The pore area ($2 \times 0.5 \mu\text{m}^2$, by image analysis) corresponds to a circular pore with diameter $\sim 1.15 \mu\text{m}$, larger than the nominal pore size provided by the manufacturer ($0.2 \mu\text{m}$). The surface and bulk porosities are 63% and 80%, respectively. The effective thickness of the membrane is $\sim 50 \mu\text{m}$, whereas the total thickness is $130 \mu\text{m}$, with a scrim type mechanical support being used. This mechanical support, as shown in Fig. 10(e), would cause at least 50% reduction of porosity as well as blockage of transport path (Adnan *et al.* 2012). Based on the SEM image analyses, both M70 and PTFE membranes have an equivalent pore diameter of $\sim 1 \mu\text{m}$. Hence, it is reasonable to claim that the influences from pore size on MD performances are much smaller than those from porosity (taking into account support usage) and membrane thickness. The former factor appears to favor higher fluxes for M70. However, it is noted that the thickness of PTFE is only $\sim 1/4$ - $1/3$ that of M70, which counterbalances the porosity factor and allow PTFE to have higher fluxes than M70 for all tested operations. Furthermore, it is worth mentioning that the permeation flux normally does not vary linearly with membrane thickness (Martinez and Rodriguez-Maroto 2008), but with an increase first then decrease or reach a plateau type of dependence. This partly explains why the flux of PTFE is higher than M70 only by $\sim 10\%$ even with a significantly smaller effective thickness.

4. Conclusions

PVDF membranes were prepared by isothermal immersion-precipitation of PVDF/TEP casting dopes in coagulation baths of different TEP contents. The formed membranes exhibited a uniform cross-section composed of interlocked crystal elements coexisting with the network of continuous pores. Morphologies of the membranes' top surfaces were found to depend on the bath strength. By changing the bath gradually from pure water to 70% TEP solution, the top surface evolved from skin to porous morphology. Membrane distillation process to separate sodium chloride from water was carried out on various prepared PVDF membranes. In the optimum case (membrane M70, with a symmetric bi-continuous structure), the permeation flux reaches 12.8 LMH at the feed temperature of 50°C , which is comparable to that of a commercial PTFE membrane (13.9 LMH) operated at the same condition. The MD performances of various membranes were compared and explained based on the structural factors: porosity, pore size, membrane thickness, and mechanical support usage.

Acknowledgments

The authors thank the National Science Council of Taiwan for the financial support (NSC 96-2628-E-032-001-MY3).

References

- Adnan, S., Hoang, M., Wang, H.T. and Xie, Z.L. (2012), "Commercial PTFE membranes for membrane distillation application: Effect of microstructure and support material", *Desalination*, **284**, 297-308.
- Akbari, A., Hamadian, M., Jabbari, V., Lehi, A.Y. and Bojaran, M. (2012), "Influence of PVDF concentration on the morphology, surface roughness, crystalline structure, and filtration separation properties of semicrystalline phase inversion polymeric membranes", *Desalination and Water Treatment*, **46**(1-3), 96-106.
- Banat, F.A. and Simandl, J. (1994), "Theoretical and experimental-study in membrane distillation", *Desalination*, **95**(1), 39-52.
- Banat, F.A. and Simandl, J. (1998), "Desalination by membrane distillation: A parametric study", *Separ. Sci. Technol.*, **33**(2), 201-226.
- Calabro, V., Jiao, B.L. and Drioli, E. (1994), "Theoretical and experimental-study on membrane distillation in the concentration of orange juice", *Ind. Eng. Chem. Res.*, **33**(7), 1803-1808.
- Chang, H.H., Chen, S C., Lin, D.J. and Cheng, L.P. (2013), "Preparation of bi-continuous Nylon-66 porous membranes by coagulation of incipient dopes in soft non-solvent baths", *Desalination*, **313**, 77-86.
- Cheng, L.P. (1999), "Effect of temperature on the formation of microporous PVDF membranes by precipitation from 1-octanol/DMF/PVDF and water/DMF/PVDF systems", *Macromolecules*, **32**(20), 6668-6674.
- Essalhi, M. and Khayet, M. (2013), "Self-sustained webs of polyvinylidene fluoride electrospun nanofibers at different electrospinning times: 1. Desalination by direct contact membrane distillation", *J. Membr. Sci.*, **433**, 167-179.
- Findley, M.E. (1967), "Vaporization through Porous Membranes", *Ind. Eng. Chem. Process Des. Develop.*, **6**(2), 226-230.
- Findley, M.E., Tanna, V.V., Rao, Y.B. and Yeh, C.L. (1969), "Mass and heat transfer relations in evaporation through porous membranes", *Aiche J.*, **15**(4), 483-489.
- Gryta, M. and Barancewicz, M. (2010), "Influence of morphology of PVDF capillary membranes on the performance of direct contact membrane distillation", *J. Membr. Sci.*, **358**(1-2), 158-167.
- Hou, D.Y., Dai, G.H., Wang, J., Fan, H., Zhang, L. and Luan, Z.K. (2012), "Preparation and characterization of PVDF/nonwoven fabric flat-sheet composite membranes for desalination through direct contact membrane distillation", *Sep. Purif. Technol.*, **101**, 1-10.
- Hou, D.Y., Wang, J., Sun, X.C., Ji, Z.G. and Luan, Z.K. (2012), "Preparation and properties of PVDF composite hollow fiber membranes for desalination through direct contact membrane distillation. *Journal of Membrane Science*, **405**, 185-200.
- Kuo, C.Y., Lin, H.N., Tsai, H.A., Wang, D.M. and Lai, J.Y. (2008), "Fabrication of a high hydrophobic PVDF membrane via nonsolvent induced phase separation", *Desalination*, **233**(1-3), 40-47.
- Lai, C.L., Liou, R.M., Chen, S.H., Huang, G.W. and Lee, K.R. (2011), "Preparation and characterization of plasma-modified PTFE membrane and its application in direct contact membrane distillation", *Desalination*, **267**(2-3), 184-192.
- Lawson, K.W. and Lloyd, D.R. (1996a), "Membrane distillation. 1. Module design and performance evaluation using vacuum membrane distillation", *J. Membr. Sci.*, **120**(1), 111-121.
- Lawson, K.W. and Lloyd, D.R. (1996b), "Membrane distillation. 2. Direct contact MD", *J. Membr. Sci.*, **120**(1), 123-133.
- Lawson, K.W. and Lloyd, D.R. (1997), "Membrane distillation", *J. Membr. Sci.*, **124**(1), 1-25.
- Liao, Y., Wang, R., Tian, M., Qiu, C.Q. and Fane, A.G. (2013), "Fabrication of polyvinylidene fluoride (PVDF) nanofiber membranes by electro-spinning for direct contact membrane distillation", *J. Membr. Sci.*, **425-426**, 30-39.
- Lin, D.J., Chang, C.L., Lee, C.K. and Cheng, L.P. (2006a), "Fine structure and crystallinity of porous Nylon 66 membranes prepared by phase inversion in the water/formic acid/Nylon 66 system", *Eur. Polym. J.*, **42**(2), 356-367.
- Lin, D.J., Chang, C.L., Lee, C.K. and Cheng, L.P. (2006b), "Preparation and characterization of

- microporous PVDF/PMMA composite membranes by phase inversion in water/DMSO solutions”, *Eur Polym. J.*, **42**(10), 2407-2418.
- Lin, D.J., Chang, H.H., Chen, T.C., Lee, Y.C. and Cheng, L.P. (2006), “Formation of porous poly(vinylidene fluoride) membranes with symmetric or asymmetric morphology by immersion precipitation in the water/TEP/PVDF system”, *Eur. Polym. J.*, **42**(7), 1581-1594.
- Martinez, L. and Rodriguez-Maroto, J.M. (2008), “Membrane thickness reduction effects on direct contact membrane distillation performance”, *J. Membr. Sci.*, **312**(1-2), 143-156.
- Pang, R.Z., Li, J.S., Wei, K.J., Sun, X.Y., Shen, J.Y., Han, W.Q. and Wang, L.J. (2011), “In situ preparation of Al-containing PVDF ultrafiltration membrane via sol-gel process”, *J. Colloid Interf. Sci.*, **364**(2), 373-378.
- Phattaranawik, J., Jiratananon, R. and Fane, A.G. (2003), “Heat transport and membrane distillation coefficients in direct contact membrane distillation”, *J. Membr. Sci.*, **212**(1-2), 177-193.
- Wang, X.Y., Zhang, L., Sun, D.H., An, Q.F. and Chen, H.L. (2009), “Formation mechanism and crystallization of poly(vinylidene fluoride) membrane via immersion precipitation method”, *Desalination*, **236**(1-3), 170-178.
- Zhang, M., Zhang, A.Q., Zhu, B.K., Du, C.H. and Xu, Y.Y. (2008), “Polymorphism in porous poly(vinylidene fluoride) membranes formed via immersion precipitation process”, *J. Membr. Sci.*, **319**(1-2), 169-175.
- Zhang, P.Y., Yang, H. and Xu, Z.L. (2012), “Preparation of polyvinylidene fluoride (PVDF) membranes via nonsolvent induced phase separation process using a tween 80 and H₂O mixture as an additive”, *Ind. Eng. Chem. Res.*, **51**(11), 4388-4396.